A new self-consistent approach for the inclusion of Madelung corrections into the Hartree-Fock-Roothaan method for solids: application to two- and three-dimensional crystals of intermediate ionicity

1991 J. Phys.: Condens. Matter 3 2621

(http://iopscience.iop.org/0953-8984/3/16/003)

J. Phys.: Condens. Matter 3 (1991) 2621–2638. Printed in the UK

A new self-consistent approach for the inclusion of Madelung corrections into the Hartree–Fock–Roothaan method for solids: application to two- and three-dimensional crystals of intermediate ionicity

P Saalfrank

Department of Theoretical Chemistry, Friedrich-Alexander-University Erlangen-Nürnberg, Egerlandstrasse 3, D-8520 Erlangen, Federal Republic of Germany

Received 22 August 1990, in final form 21 January 1991

Abstract. A new method for the self-consistent treatment of Madelung potentials within the usual Hartree–Fock–Roothaan scheme for periodic systems is presented. The new approach is based on Mulliken's population analysis and Ewald's rapid-convergence technique for the evaluation of lattice sums. The method is applied to two- and three-dimensional crystals of intermediate ionicity. We find that, while energy-related quantities are less affected, wavefunction-related observables depend strongly on the proper consideration of Madelung effects. Depending on the respective system, the Madelung potentials act to enhance or lower ionicity. The higher the crystal dimensionality, the more important are the Madelung corrections.

1. Introduction

The extent of ionicity in a given crystal may extensively fix its physical properties. So from the classical theories of Born and Landé [1] and Madelung [2] we know that the lattice energy of ionic solids can be well reproduced by considering a repulsive and an attractive term, the latter being solely determined by the Coulomb interaction between ions. Secondly, it has been emphasized that lattice dynamics is strongly governed by electrostatic interatomic potentials [3]. To give a third example let us point to surface chemistry: the catalytic activity of several metal oxides depends to a large extent on the surface Madelung potential [4].

Not only the interaction between particles with large net charges, but also more general long-range Coulomb forces that are present even in solids consisting of moderately charged subunits, may cause a surprise. Brédas [5] has shown for polyethylene that, if long-range contributions are properly handled, the zig-zag conformation in agreement with chemical intuition is more stable than a *gauche* form. Ignoring these contributions led to the opposite conclusion.

From a theoretical point of view the question arises, how to treat classical Madelung sums and (more general) long-range forces. The problem we face with lattice sums is their poor convergence, especially if two- (2D) and three-dimensional (3D) species containing highly charged ions are under consideration. Two classical, rapidly converging methods for the evaluation of Madelung sums have been proposed by Ewald [6]

0953-8984/91/162621 + 18 $03.50

and Evjen [7], respectively. In the latter method, lattice sums are analysed by grouping contributions into shells of vanishing net charge, while in the former case the original Madelung series is replaced by two quickly converging sums (see below). Improved versions of both techniques have been developed [8, 9].

Later, for instance, Metzger [10] used Ewald's method within a semiclassical framework to compute the total energies of several ionic crystals containing organic molecules. In these studies the charges of the constituents had to be presumed, i.e. different point-charge arrays had to be compared. Pisani *et al* [11], to obtain improved total energies for ionic systems, corrected their usual quantum-chemical *ab initio* calculations for the long-range Coulomb part, again applying Ewald-type summations. They took the net charges necessary for evaluating corrected total energies from a preceding *ab initio* treatment, but Madelung potentials did not enter into the Fock matrix (see below).

Some kind of self-consistency in semiempirical schemes, for example, was introduced by Wang *et al* [12] to describe properly ionic molecules and solids on the extended Hückel level [13] ('iterative extended Hückel theory'). This was managed by adjusting the empirical parameters iteratively to the respective atomic orbital occupations. There are also several quasi-self-consistent and self-consistent schemes for incorporating ionic effects in local-exchange density-functional-type computations [14, 15]. In the field of *ab initio* Hartree–Fock, linear combination of atomic orbitals, crystal orbital (HF LCAO CO) investigations of solids [16, 17], the work of the Namur polymer group has to be emphasized. To treat long-range electrostatic interactions in a self-consistent manner, two main approaches were developed, namely (i) a combination of the multipole expansion technique with the Riemann zeta function [18, 19] and (ii) the Fourier [20–22] and Laplace transform [23] methods. These different techniques were applied to one-dimensional solids (polymers).

In this work we present a new and computationally simple scheme to treat Madelung effects self-consistently in the framework of the usual HF LCAO CO technique. The ingredients for our method are Ewald's lattice summation and Mulliken's population analysis [24].

The paper is organized as follows. In section 2 the theoretical background is developed. Subsections review the usual HF LCAO CO method, describe the computation of Madelung site potentials via Ewald sums and show how Madelung matrix elements are evaluated. Section 3 gives some details concerning the computational realization. In section 4, investigations on hexagonal 2D and cubic 3D boron nitride as well as on layers of carbon monoxide molecules are presented. A final section, 5, gives several conclusions and points to some potential extensions of the method. In an appendix the approximations concerning the Madelung matrix elements are justified both numerically and analytically.

2. Method

2.1. Long-range problems in HF LCAO CO schemes

Though the standard HF LCAO CO method, which we use as a starting point for the self-consistent inclusion of Madelung potentials, is well described elsewhere [16, 17], for future reference the basic equations are reviewed.

Applying the method, the pseudo-eigenvalue problem

$$\mathbf{F}(\boldsymbol{k})\boldsymbol{c}_n(\boldsymbol{k}) = \varepsilon_n(\boldsymbol{k})\mathbf{S}(\boldsymbol{k})\boldsymbol{c}_n(\boldsymbol{k}) \tag{1}$$

has to be solved for different $\boldsymbol{k}$-vectors belonging to the first Brillouin zone (BZ) and for different CO indexed by n. In (1), $\varepsilon_n(\boldsymbol{k})$ gives the dispersion of the nth band, while $\boldsymbol{c}_n(\boldsymbol{k})$ contains the coefficients for the LCAO expansion of the nth CO as a function of quasi-momentum $\boldsymbol{k}$. Moreover $\mathbf{F}(\boldsymbol{k})$ and $\mathbf{S}(\boldsymbol{k})$ are Fock and overlap matrices in reciprocal space, respectively, their elements being related to configuration-space quantities by

$$F_{\mu\nu}(\boldsymbol{k}) = \sum_{j=0}^{N} \exp(\mathrm{i}\boldsymbol{k}\cdot\boldsymbol{R}_j) f_{\mu\nu}^{0j} \tag{2a}$$

$$S_{\mu\nu}(\boldsymbol{k}) = \sum_{j=0}^{N} \exp(\mathrm{i}\boldsymbol{k}\cdot\boldsymbol{R}_j) S_{\mu\nu}^{0j}. \tag{2b}$$

(Here Greek letters represent atomic orbital (AO) indices, and arabic letters cell indices.) In principle, for an infinite crystal the sum over lattice vectors $\boldsymbol{R}_j$ tends to infinity. The Fock matrix elements in direct space

$$f_{\mu\nu}^{0j} = T_{\mu\nu}^{0j} + Z_{\mu\nu}^{0j} + C_{\mu\nu}^{0j} + X_{\mu\nu}^{0j} \tag{3}$$

contain kinetic ($T_{\mu\nu}^{0j}$), nuclear attraction ($Z_{\mu\nu}^{0j}$), electron–electron repulsion ($C_{\mu\nu}^{0j}$) and exchange ($X_{\mu\nu}^{0j}$) terms, the Coulomb interaction terms $Z_{\mu\nu}^{0j}$ and $C_{\mu\nu}^{0j}$ being given by

$$Z_{\mu\nu}^{0j} = -\sum_{h=0}^{M}\sum_{B=1}^{K_B} \left\langle \chi_\mu^0(\boldsymbol{r}) \left| \frac{Z_B}{|\boldsymbol{r}-\boldsymbol{R}_h-\boldsymbol{R}_B|} \right| \chi_\nu^j(\boldsymbol{r}) \right\rangle \tag{4a}$$

$$C_{\mu\nu}^{0j} = \sum_{h,l=0}^{M}\sum_{\sigma,\lambda} P_{\sigma\lambda}^{0h} \left\langle \chi_\mu^0(\boldsymbol{r}_1)\chi_\sigma^h(\boldsymbol{r}_2) \left| \frac{1}{|\boldsymbol{r}_1-\boldsymbol{r}_2|} \right| \chi_\nu^j(\boldsymbol{r}_1)\chi_\lambda^l(\boldsymbol{r}_2) \right\rangle. \tag{4b}$$

Here, χ_α^a is the AO α in cell a characterized by the lattice vector $\boldsymbol{R}_a$; Z_B is the nuclear charge of atom B (K_B atoms per cell); and $P_{\sigma\lambda}^{0h}$ represents an element of the density matrix, calculated from LCAO coefficients by integration over the occupied part of the first BZ. Again, as in the case of equations (2), the summation over lattice indices h and l in (4) has to be performed to infinity. In practice only lattice vectors up to $\boldsymbol{R}_M$ are considered, which we call the 'Madelung radius'.

As shown elsewhere [25], the Fourier expansion (equations (2)) converges very rapidly for overlap, kinetic and exchange terms. However, the electrostatic summations (4*a*) and (4*b*) individually diverge. Combining both leads to a conditionally convergent series, but convergence is very slow owing to the delicate balance between negative (nuclear attraction) and positive (electron–electron) contributions. The situation even deteriorates for (i) ionic or partially ionic solids with large effective atom charges and (ii) systems of dimensionality higher than 1 [26]. In these cases, owing to the computational effort in treating many-neighbours interactions, only simple systems can properly be handled on the *ab initio* level.

2.2. *Madelung site potentials*

The above-mentioned lattice summations of electrostatic interactions in quantum chemistry perfectly match the classical Madelung problem. We shall adopt Ewald's rapid-convergence technique to correct the Coulomb integrals of equations (4*a*) and (4*b*) for

their long-range part, i.e. we shall perform, as usual, the lattice sums explicitly only up to a (not too large) number M, and then add 'external' Madelung matrix elements.

If K_B again is the number of atoms per unit cell and each atom B is carrying an effective charge Q_B, then

$$\tilde{V}^{\mathrm{M}}(\boldsymbol{R}_A) = \sum_{h=0}^{\infty} \sum_{B=1}^{K_B} \frac{Q_B}{|\boldsymbol{R}_A - \boldsymbol{R}_B - \boldsymbol{R}_h|} := \sum_B \tilde{M}_{AB} Q_B \tag{5}$$

is the total Madelung potential at site $\boldsymbol{R}_A$ (M_{AB} is a short-hand notation for the lattice sum 'pair potential factors'). Since the short-range electrostatic contributions are already included in the standard HF treatment (summation up to M in (4)), an 'external' Madelung site potential $V^{\mathrm{M}}(\boldsymbol{R}_A)$ should be defined as

$$V^{\mathrm{M}}(\boldsymbol{R}_A) = \sum_{h=M+1}^{\infty} \sum_{B=1}^{K_B} \frac{Q_B}{|\boldsymbol{R}_A - \boldsymbol{R}_B - \boldsymbol{R}_h|} := \sum_B M_{AB} Q_B. \tag{6}$$

The external pair potential factors M_{AB}, as can easily be proven, are all infinite. However, since they all contain the same infinite constant term, owing to the unit-cell charge neutrality constraint $V^{\mathrm{M}}(\boldsymbol{R}_A)$ stays finite. Consequently, this singular term is omitted in actual calculations, and M_{AB} may be evaluated using Ewald's technique as [27]

$$M_{AB} = \frac{4\pi}{v_0} {\sum_{\mu}}' \frac{1}{k_\mu^2} \exp\left(-\frac{k_\mu^2}{4\varepsilon^2} + \mathrm{i}\boldsymbol{k}_\mu \cdot (\boldsymbol{R}_A - \boldsymbol{R}_B) \right) + \sum_h \frac{1}{|\boldsymbol{R}_A - \boldsymbol{R}_B - \boldsymbol{R}_h|} \operatorname{erfc}(\varepsilon |\boldsymbol{R}_A - \boldsymbol{R}_B - \boldsymbol{R}_h|). \tag{7}$$

The reason Ewald's method improves convergence is given by the fact that a slowly convergent series has been replaced by two rapidly converging sums, the first one running over reciprocal lattice vectors $\boldsymbol{k}_\mu$, the second one over direct lattice vectors $\boldsymbol{R}_h$ multiplied by the quickly decreasing function $\operatorname{erfc}(u)$, the so-called complementary error function:

$$\operatorname{erfc}(u) = \frac{2}{\sqrt{\pi}} \int_u^{\infty} \exp(-t^2)\, \mathrm{d}t.$$

In equation (7), v_0 is the volume of the reference cell and ε is an arbitrary parameter, which may be chosen to optimize convergence. The prime on the reciprocal sum indicates that the infinite constant term has to be omitted. In actual calculations attention must be paid to the cases $\boldsymbol{R}_A - \boldsymbol{R}_B = 0$ or $\boldsymbol{R}_A - \boldsymbol{R}_B = \boldsymbol{R}_j$ ($\boldsymbol{R}_j$ being an arbitrary lattice vector)—then an additional singular term will occur in the direct lattice sum of equation (7). This term is also omitted and, as shown in [27], leads to a correction term $-2\varepsilon/\sqrt{\pi}$.

To extract Madelung potentials from equation (6) the net charges Q_B must be known. Since the Madelung site potentials depend on these charges and vice versa, a self-consistent scheme is required. To proceed, let Q_B be

$$Q_B = -Z_B + N_B \tag{8}$$

where Z_B is the nuclear charge of atom B and N_B is the number of electrons associated with it. N_B can be determined by Mulliken's population analysis as

$$N_B = \sum_{\sigma \in B} q_\sigma \tag{9a}$$

$$q_\sigma = \sum_h \sum_\lambda P_{\sigma\lambda}^{0h} S_{\sigma\lambda}^{0h}. \tag{9b}$$

Here q_σ counts the electron attributed to the atomic orbital χ_σ. This number, similar to the molecular case, results from summing products of density and overlap matrix elements over all AO indices λ. Additionally to the molecular situation a sum over lattice indices h has to be performed.

2.3. Madelung matrix elements

Using equations (8) and (9) in equation (6) enables us to compute 'external' Madelung site potentials

$$V^{\mathrm{M}}(\boldsymbol{R}_A) = \sum_{B=1}^{K_B} M_{AB} \left(-Z_B + \sum_h \sum_{\sigma \in B} \sum_\lambda P_{\sigma\lambda}^{0h} S_{\sigma\lambda}^{0h} \right) \tag{10}$$

with M_{AB} given by equation (7). To incorporate these in the usual HF framework, a prescription must be given for how to define matrix elements. The best way, of course, would be to determine the potential as a continuous function of space, $V^{\mathrm{M}}(\boldsymbol{r})$, and then to integrate analytically or numerically. Fortunately, this formidable task can be circumvented by noting that the Madelung matrix elements $V_{\mu\nu}^{0j,\mathrm{M}}$ can be well approximated simply from atomic site interaction site potentials, respectively, and overlap matrix elements according to

$$V_{\mu\nu}^{0j,\mathrm{M}} = \begin{cases} V^{\mathrm{M}}(\boldsymbol{R}_A) S_{\mu\nu}^{0j} & \text{if} \quad \mu, \nu \in A \qquad (11a) \\ V^{\mathrm{M}}(\boldsymbol{R}_{\mathrm{H}}) S_{\mu\nu}^{0j} & \text{if} \quad \mu \in A, \nu \in B. \qquad (11b) \end{cases}$$

Here, $\boldsymbol{R}_{\mathrm{H}} = (\boldsymbol{R}_A + \boldsymbol{R}_B + \boldsymbol{R}_j)/2$ is the midpoint between the centres of atomic orbitals χ_μ^0 and χ_ν^j. Our approximate treatment of the three-centre-like integrals via equation (11*b*) is similar to the well known Mulliken approximation [28] in the sense that proportionality to the overlap is assumed. However, while Mulliken computes intersite potentials by averaging atomic site potentials, we use potentials at intersite positions without reference to site Madelung potentials.

The evaluation of Madelung potentials via equations (6) or (10) ultimately has its basis in the point-charge approximation, which works well if the charges are well apart from the AO centres. The approximations concerning 'diagonal' (equation (11*a*)) and 'off-diagonal' (equation (11*b*)) matrix elements go beyond this and are examined in detail in the appendix. To prevent us from loss of continuity, the main results are summarized: (i) the exact (with respect to the point-charge approach) diagonal matrix elements are matched by equation (11*a*) within less than 10^{-5} eV if the point charges are about 4 Å away from atom A; (ii) the 'exact' off-diagonal elements are non-negligible and are approximated by equation (11*b*) to roughly 10^{-4} eV if the point charges are about 8 Å apart from the midpoint between centres A and B. Furthermore the appendix shows how equation (11*b*) could be improved further by computing the Madelung potentials at 'weighted' midpoints between AO centres rather than at the geometrical ones. In short, the additional approximations (11*a*) and (11*b*) match the requirements necessary for the point-charge approximation.

In the next section we shall see that the computational procedure we use in actual calculations meets all the requirements concerning distances between point charges and either atoms or midpoints between atoms. As a consequence, equations (10) and (11) are good representations of the 'true' external Madelung potentials and elements, respectively. Note that this is accomplished without additionally complicated computations: the $S_{\mu\nu}^{0j}$ have to be evaluated anyhow, and the site potentials are easily

calculated if a population analysis has been performed and once the external pair potential factors have been determined.

As soon as the Madelung matrix elements are known, the original Fock matrix may be corrected as

$$\mathbf{F}^{\mathrm{M}}(\mathbf{P}) = \mathbf{F}(\mathbf{P}) + \mathbf{V}^{\mathrm{M}}(\mathbf{P}) \tag{12}$$

to yield the new matrix $\mathbf{F}^{\mathrm{M}}$. We stress that the Madelung matrix $\mathbf{V}^{\mathrm{M}}$ depends on the same density matrix $\mathbf{P}$ as the usual electron–electron interaction does. Thus self-consistency for both terms is achieved simultaneously. Self-consistency is not restricted to the evaluation of Madelung potentials with the help of Mulliken populations. Any $\mathbf{P}$-dependent alternative scheme could have been used, for instance Löwdin's technique to start from orthogonalized atomic orbitals [29].

3. Computational details

For our HF LCAO CO calculations we use the program package CRYSTAL developed by Pisani *et al* [11, 30] and modified by our group [31, 32]. In the original version of CRYSTAL, long-range Coulomb forces enter into the computational scheme as a classical Madelung correction to the quantum-mechanical total energy [11]:

$$E^{\mathrm{tot}} = \tfrac{1}{2}\,\mathrm{Tr}[\mathbf{P}(\mathbf{H} + \mathbf{F})] + V_{\mathrm{NN}} + E^{\mathrm{Mad}}(\boldsymbol{R}_{\mathrm{M}}) \tag{13}$$

where

$$E^{\mathrm{Mad}}(\boldsymbol{R}_{\mathrm{M}}) = \tfrac{1}{2}\sum_{A,B}^{K_B} M_{AB} q_A q_B \tag{14}$$

is the external Madelung energy arising from Coulomb interactions between cells with distances larger than the Madelung radius $\boldsymbol{R}_{\mathrm{M}}$, and V_{NN} is the nucleus–nucleus interaction energy for nuclei within the HF zone. Note that the net charges q_A and q_B in (14) differ from our effective charges Q_B (equations (8) and (9)) in that they result from wavefunctions obtained by diagonalizing Madelung-uncorrected Fock matrices. Thus a 'quantum' zone is separated from a 'classical' zone by the Madelung radius $\boldsymbol{R}_{\mathrm{M}}$. The quantum zone itself in CRYSTAL is further partitioned into a 'bielectronic' zone, where two-electron integrals are evaluated exactly, and a 'monoelectronic' one, where these are approximated via a multipole expansion as one-electron integrals. The basic features are graphically displayed in figure 1.

In the present work the 'quantum' zone in an approximate way is extended to infinity. Since the major contributions to the Madelung potentials originate from point charges lying deep in the Madelung region or at least far away from AO centres, the requirements for the applicability of equations (11) are fulfilled. Problems might arise if the lattice vector $\boldsymbol{R}_j$ pointing to the cell where AO χ_ν^j is located obeys the condition $|\boldsymbol{R}_j| \approx |\boldsymbol{R}_{\mathrm{M}}|$, i.e. the atomic orbital χ_ν^j comes close to strongly contributing point charges. In this case, however, the corresponding matrix elements are small owing to the small overlap between χ_μ^0 and χ_ν^j—hence the error is negligible.

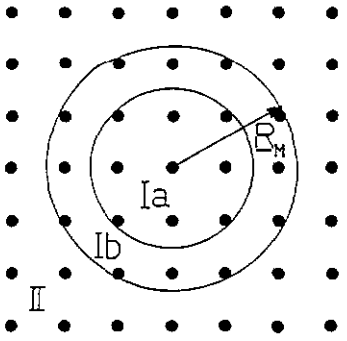

Figure 1. Evaluation of Coulomb integrals in CRYSTAL: Ia, bielectronic zone; Ib, monoelectronic zone; II, Madelung zone with Madelung radius R_M.

4. Applications

We are now in the position to apply the formalism to selected systems. In choosing appropriate model compounds, we were guided by the following considerations: neither fully non-ionic nor fully ionic species should be good candidates, since in the first case the external Madelung potential is zero, while in the second it will not be able to increase ionicity further. Larger differences, especially in the charge distributions, are to be expected for species of intermediate ionicity. Moreover, the model systems should be simple enough to allow for detailed investigations, but they should be realistic enough to make comparisons possible with experiment and other calculations, respectively. Thus boron nitride in hexagonal (2D) and cubic (3D) modifications as well as carbon monoxide layers were studied.

4.1. Hexagonal boron nitride (HBN)

The most important modifications of solid BN are the hexagonal (henceforth HBN) and cubic (CBN) forms. These are the crystallographic analogues to graphite and diamond, respectively. As may be seen from figure 2(*a*), HBN consists of honeycomb-like layers, which are weakly coupled with neighbouring layers mainly through van der Waals type interactions. Thus, similar to graphite, HBN can be idealized as a 2D system while CBN (figure 2(*b*)) clearly cannot.

Both HBN and CBN have been investigated theoretically on the HF LCAO CO level [33, 34] using the local-exchange approximation [35] or semiempirical schemes [36]. Dovesi *et al* [33] computed cohesive energies and equilibrium lattice parameters for HBN and CBN by applying a standard STO-3G (Slater-type orbitals, three Gaussian) basis set [37]. The theoretical binding energies were about 3.2 eV too small compared with experiment (E_B = 13 eV/cell) while the calculated lattice parameters agreed to within less than 0.1 Å with measured values. The positive net charges on boron were 0.50 and 0.21 for HBN and CBN, respectively.

In our own work we performed analogous calculations with somewhat improved truncation criteria. Calculations without and with Madelung corrections were compared.

Let us first consider energetics in the form of potential curves. For HBN, three curves representing three different methods are displayed in figure 3(*a*). These three curves refer to the following cases: (1) no Madelung correction, (2) Madelung correction to

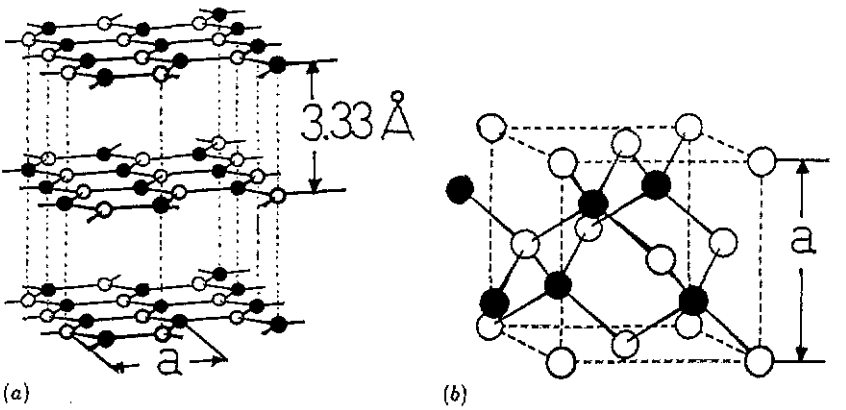

Figure 2. Crystal structures of (*a*) hexagonal and (*b*) cubic boron nitride (HBN and CBN, respectively).

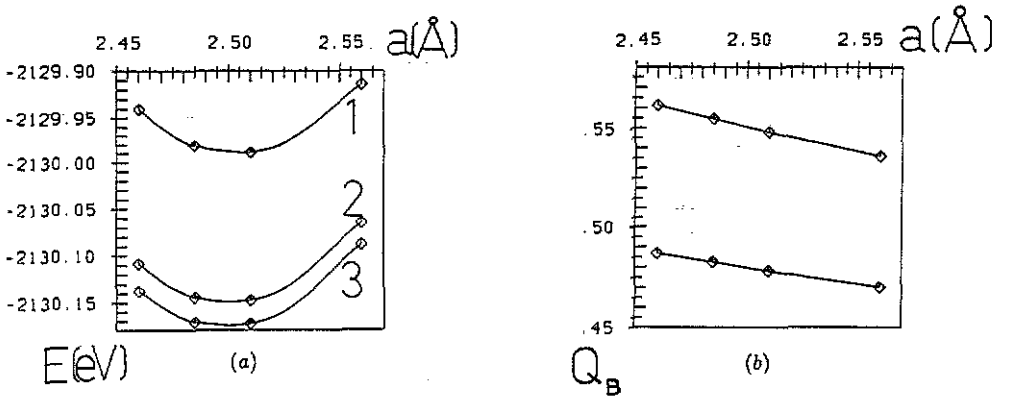

Figure 3. (*a*) STO-3G potential curves for HBN: 1, no Madelung correction; 2, Madelung correction to total energy; 3, Madelung correction to total energy and Fock matrix. (*b*) Net charge on *B* without (lower curve) and with (upper curve) Madelung correction.

only the total energy (equation (13)) and (3) Madelung correction to both the Fock matrix and the total energy. First of all we mention that the computed minima match the experimental one (2.51 Å) fairly well. More importantly from figure 3 we realize: (i) the Madelung correction to only the total energy is negative (−0.16 eV at a lattice parameter of 2.51 Å and $|R_M| = 12.55$ Å); (ii) the Madelung correction to the Fock matrix further stabilizes the systems. Probably because of the less restricted truncations we use, in comparison to [33] our binding energies are somewhat closer to experiment (about 11.4 against about 9.8 eV at 2.51 Å for curve 2), but are still too small. Thus curve 3 has to be preferred to curve 2, and curve 2 has to be preferred to curve 1, i.e. the successive improved inclusion of Madelung effects successively improves binding energies. However, while the difference between curves 1 and 2 is important, case 3 only brings a very small additional energy lowering (0.03 eV at 2.51 Å).

Are there more significant changes in the wavefunction 'measured' by calculated effective charges? Figure 3(*b*) gives positive effective charges on boron in HBN for

Table 1. Total energies (eV) for HBN obtained with Clementi's MB for different lattice vectors (row 1). The energies E_1, E_2 and E_3 correspond to the cases 1, 2 and 3 of figure 3. Rows 5 and 6 give uncorrected (Q_B^0) and corrected (Q_B^M) charges on B (in units of $|e|$).

a (Å)	2.46	2.485	2.51	2.56
E_1	−2151.1186	−2151.2055	−2151.2594	−2151.2658
E_2	−2151.4190	−2151.5052	−2151.5576	−2151.5562
E_3	−2151.5864	−2151.6495	−2151.2594	−2151.6629
Q_B^0	0.652	0.654	0.656	0.653
Q_B^M	0.775	0.773	0.770	0.761

different lattice spacings, obtained via Mulliken's analysis. One immediately recognizes that ionicity increases if Madelung potentials are considered in a self-consistent manner. This is due to the fact that for HBN the Madelung potential acts in a stabilizing fashion—thus the more ionic species will be preferred. A closer examination shows that the smaller the B–N distances, the larger is the charge separation between both kinds of atoms. In parallel, an increasing Madelung correction to the total energy can be observed. This is simply because the Madelung potentials in absolute values are large for small lattice constants, since the pair potential factors are large. Since HBN becomes more ionic by about 15% due to the external Madelung potential, we may conclude that the exact evaluation of strongly wavefunction-dependent quantities (charge distribution, form factors, bond orders, dipole moments, etc) requires the inclusion of Madelung effects already for species of moderate ionicity.

To gain some more realistic insights into the significance of Madelung effects, the above calculations were repeated with Clementi's minimal basis (MB) set [38] (contraction schemes for both B and N: (73)/[21]), which usually yields total energies nearly of double-zeta quality. Table 1 shows total energies (rows 2–4) and charge distributions (rows 5 and 6), respectively.

Compared to Pople's STO-3G, the total energies appear to be lower by about 21 eV. However, these absolute values are much less interesting than the changes due to Madelung corrections, which as before are introduced step by step, i.e. the original potential curve (row 2) is first, then only energy-corrected (row 3) and then also Fock-matrix-corrected (row 4). We recognize (row 3 versus row 2) that the external Madelung energy again is negative, but somewhat larger than in the STO-3G case (−0.30 against −0.16 eV at 2.51 Å). This is because Clementi's basis predicts more ionic species already without Madelung corrections—in turn the latter become more important. Consequently total energies (row 4 versus row 2) and charge distributions (row 6 versus row 5) change more dramatically than before.

Since the Madelung technique improves total energies only by a small amount and since any charge partitioning scheme is somewhat arbitrary, an unambiguous criterion for the quality of the method is required. This criterion can be extracted from recalling figure 1: if the Madelung radius $|\boldsymbol{R}_M|$ is extended to infinity, the 'external' Madelung matrix elements will become so small that the difference between corrected and uncorrected Fock matrices must vanish. Thus, with respect to both total energies and net charges, the same limiting values must result. Figures 4(*a*) and (*b*) give total energies and boron net charges, respectively, for uncorrected and corrected calculations as a function of the Madelung radius $|\boldsymbol{R}_M|$ (the lattice parameter is fixed at 2.51 Å).

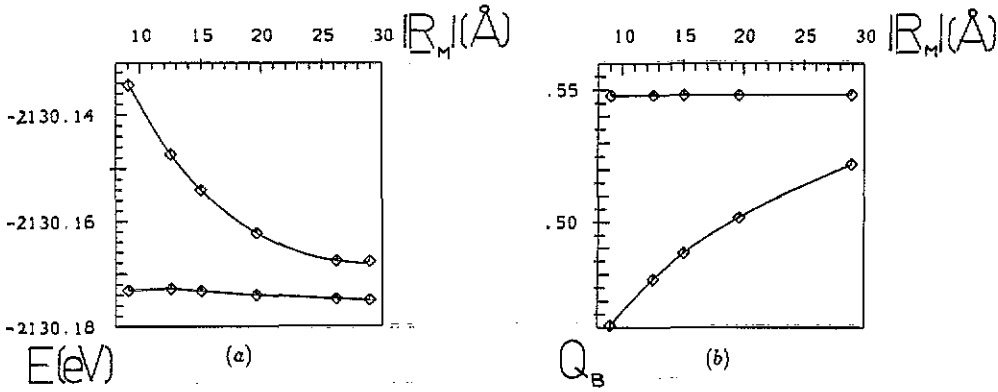

Figure 4. (*a*) Dependence of total energies on $|\boldsymbol{R}_M|$ without (upper curve) and with (lower curve) Madelung correction. (*b*) Dependence of boron net charges on $|\boldsymbol{R}_M|$ without (lower curve) and with (upper curve) Madelung correction.

We recognize that Madelung-uncorrected total energies and net charges significantly decrease and increase, respectively, with increasing $|\boldsymbol{R}_M|$. However, if Madelung potentials are considered self-consistently, these quantities show only small variations if the Madelung radius is enlarged. More importantly, the corrected curves appear to be close to the exact, i.e. converged values from the beginning, even for small $|\boldsymbol{R}_M|$. Thus the more ionic picture is the more realistic one. Since the computational effort closely parallels increasing $|\boldsymbol{R}_M|$, we conclude that more realistic band structures are obtained with less computing time if our self-consistent Madelung technique is adopted. Moreover, since for instance the effective charges appear to be very sensitive to $|\boldsymbol{R}_M|$, finite point-charge environments with fixed charges seem to be inadequate to describe the real effects properly. Both the long-range behaviour of ionic forces (because of their comparatively weak dependence on distances) and the self-consistent determination of effective charges (because the potential is proportional to them) are of importance.

4.2. Cubic boron nitride (CBN)

For 3D solids the practical difficulties associated with large Madelung radii are more serious than in 2D. On the other hand—at least for ionic and medium ionic crystals—Madelung effects are more important. Thus it is to be expected that the power of a self-consistent Madelung scheme will fully develop.

Figure 5(*a*) for CBN shows the same three potential curves as figure 3(*a*) did for HBN. These curves again were computed using Pople's STO-3G. Similar to HBN, the experimental lattice parameter (3.62 Å) is reproduced fairly well in all cases. More important for our purposes, we note that the (external) Madelung energy (curve 2 versus curve 1) is negative, but twice as large as for HBN (−0.29 and −0.16 eV at the experimental lattice parameters of 3.62 and 2.51 Å, respectively). Thus Madelung corrections are more important to 3D than to 2D systems. If one takes the Madelung potentials self-consistently into account (curve 3), this further lowers the total energy—as in 2D. But now compared to HBN an additional 'energy gain' larger by a factor of 6 (0.17 versus 0.03 eV at 3.62 and 2.51 Å, respectively) is found with Pople's STO-3G. This is simply because Madelung corrections enter in the form of a threefold sum in 3D, while in 2D only a twofold sum contributes (see equation (6)).

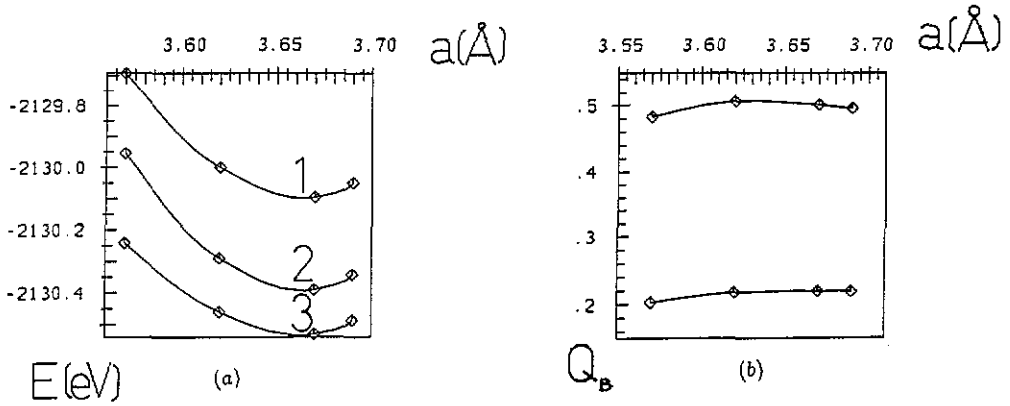

Figure 5. As figure 3, but for CBN.

Table 2. External Madelung energies (meV) for different coverages of CO layers of hexagonal symmetry. Row 2: Madelung-corrected case; row 3: Madelung-uncorrected case.

θ	1/3	7/12	1/1
E^{Mad} (corr.)	18.2	37.3	54.9
E^{Mad} (uncorr.)	19.0	41.4	66.7

The wavefunctions 'measured' via effective charges change even more dramatically owing to the self-consistent Madelung potentials. While for CBN the net charge on B increases from +0.22 to +0.51 (at 3.62 Å), the corresponding values for HBN were +0.48 and +0.56, respectively (at 2.51 Å). Thus, the Madelung potential produces comparable effective charges for 2D and 3D boron nitrides. This seems to be reasonable, since the large 3D Madelung potential compensates for the fact that the equilibrium B–N distance is larger for CBN than for HBN (1.56 versus 1.45 Å).

4.3. Layers of carbon monoxide

Up to now we have considered systems that became more ionic due to a stabilizing Madelung potential. Layers of parallel oriented carbon monoxide molecules are examples where the Madelung potentials act in a destabilizing manner. Clearly those layers are models of chemisorption and catalytic processes. To be specific, we consider hexagonal arrangements of CO molecules. If molecule–molecule separations of 4.35, 3.29 and 2.51 Å are chosen, this corresponds to the real situations of CO adsorbed on Co(0001) for the three coverages $\theta_1 = 1/3$, $\theta_2 = 7/12$ and $\theta_3 = 1/1$, respectively. While the first two coverages have been observed experimentally, the 'dense phase' θ_3 is hypothetical [39]. Theoretically all three coverages have been investigated [39, 40]. These investigations mainly focused on the interaction between metal surface and adsorbate molecules. However, we are more interested in the interaction between adsorbate molecules, especially via long-range Coulomb forces. Thus we omit the surface and take only carbon monoxide molecules into account, the C–O distance being fixed at 1.15 Å.

Applying Clementi's minimal basis (MB) (contraction scheme for both C and O: (73)/[21]), the external Madelung energies given in table 2 were computed (for the three

Table 3. Effective charges on C (in units of $|e|$) for different coverages of CO layers of hexagonal symmetry. Q_C^M: Madelung-corrected case; Q_C^0: Madelung-uncorrected case; Q_C(cluster): cluster calculation.

θ	1/3	7/12	1/1
Q_C^M	+0.329	+0.310	+0.251
Q_C^0	+0.338	+0.327	+0.277
Q_C(cluster)	+0.367	+0.364	+0.355

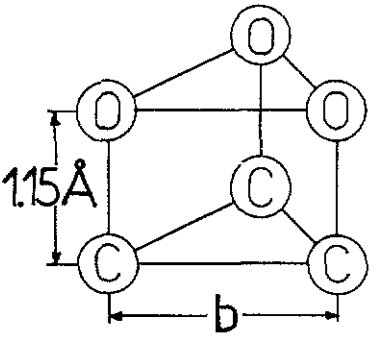

Figure 6. Cluster model for adsorption of CO.

coverages the number of internal, i.e. HF, lattice vectors was constant: $M = 91$ in equations (4*a*) and (4*b*)). The values in the second row were obtained from equation (14) with self-consistently corrected net charges, while the third row arises from effective charges calculated without Madelung correction. We recognize that the Madelung energies (i) are positive, (ii) are larger for the unmodified Fock matrices and (iii) act in a more destabilizing manner the smaller the CO–CO distances, i.e. the larger the coverage. To understand this we refer to table 3, where effective charges on carbon are listed. The second and third rows correspond to Madelung corrected and uncorrected band-structure calculations, respectively. The fourth row results from a cluster model for CO chemisorbed on Co(0001). This model consists of three parallel CO molecules, arranged in an equilateral triangle (see figure 6) with edge lengths b of 4.35, 3.29 and 2.51 Å to simulate θ_1, θ_2 and θ_3, respectively. We note that the system is most ionic in the case of the cluster ($Q_c > +0.35$ for all coverages). Taking into account more-neighbour interactions via the usual HF LCAO CO calculation (row 3) significantly lowers the charge separation between carbon and oxygen. If now, additionally, the external Madelung potential is 'switched on' (row 2), the net charges are diminished further. Thus, the destabilizing Madelung effects, in contrast to boron nitride, tend to lower ionicity. These effects appear more clearly, the more neighbours are explicitly or approximately taken into account or the smaller the lattice parameters. There is a very simple physical interpretation for the behaviour sketched above: from figure 6 one realizes that the intermolecular C–C distances are always smaller than the intermolecular C–O distances. This is true for any molecule–molecule separation. Thus, net charges of the same sign destabilize more strongly than net charges of opposite sign stabilize—the overall Coulomb interaction is positive, and the more positive the smaller the intermolecular separations. To lower the total energy, higher coverages will produce

less ionic species. If Madelung potentials are considered properly, i.e. if long-range Coulomb forces are allowed to act more effectively, the charge separation in CO layers is small for any θ.

5. Conclusion and future aspects

In conclusion, we have shown that the Ewald method in connection with an appropriate density-matrix-dependent population analysis (here Mulliken's technique) provides a promising way of treating long-range Coulomb interactions in ionic or partially ionic crystals within the usual HF LCAO CO scheme. Apart from the external pair potential factors with respect to ordinary calculations no new quantities have to be computed. Thus our scheme treats important effects in a computationally simple and economic way, especially in the case of 3D solids.

For the species we treated in this work (2D and 3D, intermediate ionicity) it turned out that mainly the wavefunctions are influenced by the Madelung potentials, while energy-related quantities are less affected. These systems become more and less ionic, respectively, in the cases of stabilizing and destabilizing potentials. For 3D species or if better basis sets were used, these effects were even more distinct.

It should be noted that the above scheme bears potentially interesting extensions and applications. So it seems possible to use self-consistent Madelung potentials instead of hundreds and thousands of fixed point charges to perform calculations on clusters modelling ionic solids. Secondly, surface Madelung potentials should be easily obtained by first halving the bulk pair potential factors and then adding half of the 2D pair potential factors. Thus—neglecting relaxation and charge-transfer effects—slab calculations might be replaced by 'single layer plus Madelung potential' computations in the case of ionic species, such as for instance metal oxides. Caution should be exercised if long-range dipole effects are of importance—they are not accounted for correctly by this crude approximation. Moreover, since pair potential factors are purely geometry-dependent, i.e. lattice-dependent, quantities, by defining average effective charges it is possible to include doping effects approximately. These average charges are simply determined by the respective doping value(s) and give rise to modified Madelung potentials. Last but not least it makes sense to treat only a subunit of a crystal explicitly, while the rest is considered via an appropriate Madelung potential.

These lines of research are in progress in our laboratory. As an example, the band structure of a single CuO_2 plane, modelling the 3D high-T_c superconductor $La_{2-x}Sr_xCuO_4$, has been determined at different doping values x, taking charge-transfer effects and a (fixed) 3D Madelung potential into account [41].

Acknowledgments

The author thanks Professors J Ladik and R F Wood for very fruitful discussions on the subject. He is indebted to Professor P Otto for making his cluster programs available.

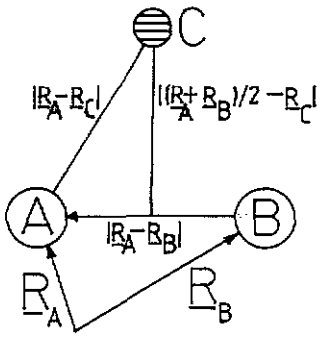

Figure 7. Cluster model used for numerical justification of equations (11*a*) and (11*b*).

Financial support of the 'Fonds der Chemischen Industrie', the 'Deutsche Forschungsgemeinschaft' (Project No. La 371/24-1) and the 'Studienstiftung des Deutschen Volkes' is gratefully acknowledged.

Appendix

Here we examine the quality of the approximation of Madelung matrix elements by products of site and intersite potentials (equations (11*a*) and (11*b*)). We use simple clusters plus point charges as models, since the Madelung technique as a whole is based on the point-charge approach.

A.1. Numerical results

Let us consider the arrangement given in figure 7, consisting of two atoms A and B at positions $\boldsymbol{R}_A$ and $\boldsymbol{R}_B$, respectively, and a single point charge C (at $\boldsymbol{R}_C$) carrying one positive elementary charge ($Q_C = +|e|$). The distance between A and C is $|\boldsymbol{R}_A - \boldsymbol{R}_C|$, while C is away from the midpoint between A and B by $|(\boldsymbol{R}_A + \boldsymbol{R}_B)/2 - \boldsymbol{R}_C|$.

According to equation (11*a*) the approximated 'diagonal Madelung matrix element' (the 'Madelung' potential is caused by the single point charge in our example) is

$$V^{\mathrm{M}}_{\mu\nu} = V^{\mathrm{M}}(\boldsymbol{R}_A)S_{\mu\nu} = -(Q_C/|\boldsymbol{R}_A - \boldsymbol{R}_C|)S_{\mu\nu} \tag{A1}$$

with $\mu, \nu \in \mathrm{A}$, while the exact matrix element is

$$\bar{V}^{\mathrm{M}}_{\mu\nu} = \left\langle \chi_\mu(\boldsymbol{r} - \boldsymbol{R}_A) \left| \frac{-Q_C}{|\boldsymbol{r} - \boldsymbol{R}_C|} \right| \chi_\nu(\boldsymbol{r} - \boldsymbol{R}_A) \right\rangle. \tag{A2}$$

Both the exact (column 2) and approximated (column 3) matrix elements are listed in table 4 for different distances $|\boldsymbol{R}_A - \boldsymbol{R}_C|$ (column 1) for the special case of A = hydrogen and $\mu = \nu = 1\mathrm{s}$ (Clementi's MB used).

Table 4. Exact ($\tilde{V}^{M}_{\mu\nu}$, column 2) and approximated ($V^{M}_{\mu\nu}$, column 3) '*diagonal* Madelung matrix elements' for $\mu = \nu =$ H 1s and different $|\boldsymbol{R}_A - \boldsymbol{R}_C|$ (energies in eV). Column 4 gives the error.

$\lvert\boldsymbol{R}_A - \boldsymbol{R}_C\rvert$ (Å)	$\tilde{V}^{M}_{\mu\nu}$	$V^{M}_{\mu\nu}$	Δ
0.65	−17.89647	−22.29130	4.30483
1.12	−12.26888	−12.84119	0.57231
1.63	−8.75966	−8.83275	0.07309
2.15	−6.69295	−6.70068	0.00773
2.67	−5.38886	−5.38943	0.00057
4.25	−3.38830	−3.38830	$<10^{-5}$
5.30	−2.71436	−2.71436	$<10^{-5}$

Table 5. Same as table 4, but for *off-diagonal* element $\mu =$ H 1s, $\nu =$ Li 2s and different $|(\boldsymbol{R}_A + \boldsymbol{R}_B)/2 - \boldsymbol{R}_C|$.

$\lvert(\boldsymbol{R}_A + \boldsymbol{R}_B)/2 - \boldsymbol{R}_C\rvert$ (Å)	$\tilde{V}^{M}_{\mu\nu}$	$V^{M}_{\mu\nu}$	Δ
1.06	−5.07804	−5.21512	0.13708
2.12	−2.59140	−2.60756	0.01616
4.23	−1.30173	−1.30377	0.00204
7.94	−0.69503	−0.69535	0.00033
13.23	−0.41713	−0.41721	0.00008

We recognize that the error (column 4) drops below 10^{-5} eV for distances $|\boldsymbol{R}_A - \boldsymbol{R}_C|$ larger than 4 Å. Using a double-zeta basis did not lead to a different conclusion. The 'off-diagonal' matrix elements in the approximation (11*b*) are

$$V^{M}_{\mu\nu} = V^{M}\left(\frac{\boldsymbol{R}_A + \boldsymbol{R}_B}{2}\right) S_{\mu\nu} = -\frac{Q_C}{|(\boldsymbol{R}_A + \boldsymbol{R}_B)/2 - \boldsymbol{R}_C|} S_{\mu\nu} \tag{A3}$$

($\mu \in A$, $\nu \in B$), while the exact elements are given by the following expression:

$$\tilde{V}^{M}_{\mu\nu} = \left\langle \chi_\mu(\boldsymbol{r} - \boldsymbol{R}_A) \left| \frac{-Q_C}{|\boldsymbol{r} - \boldsymbol{R}_C|} \right| \chi_\nu(\boldsymbol{r} - \boldsymbol{R}_B) \right\rangle. \tag{A4}$$

We introduced some asymmetry by choosing $A =$ hydrogen and $B =$ lithium ($R_{AB} =$ 0.77 Å). The values for the exact (column 2) and approximated (column 2) matrix elements between a H 1s and a Li 2s function (Clementi's MB used) are displayed in table 5 for different distances $|(\boldsymbol{R}_A + \boldsymbol{R}_B)/2 - \boldsymbol{R}_C|$.

From there we see that the matrix elements are smaller with respect to the diagonal ones, but non-negligible. Moreover, column 4 of table 5 shows us that the error decreases more slowly than in the diagonal case, but becomes about 10^{-4} eV and smaller for distances of 8 Å and above. Besides the discussed matrix element others were considered, other basis sets were used and more point charges were introduced. The result was that approximation (A3) and hence (11*b*) turned out to be stable against all these variations. Especially, owing to symmetry, exact elements that are zero are also zero in the aproximated case. Since in actual calculations we use Madelung radii $|\boldsymbol{R}_M|$ of the order of magnitude of 10 Å and more, from the above numerical investigations

the conclusions may be drawn that (i) the Madelung (point-charge) approximation is justified and (ii) the additional approximations (11*a*) and (11*b*) are accurate within about 10^{-5} eV.

A.2. Analytical results

Numerically the validity of equations (11) has been justified. We now want to show analytically why these equations work and how the approximation for the non-diagonal elements can be further improved.

Since in our quantum-chemical treatment of molecules and solids Gaussian-type expansions of Slater functions are used, let us restrict ourselves for simplicity to single, unnormalized, s-type Gaussian basis functions:

$$\chi_\mu(\boldsymbol{r}-\boldsymbol{R}_A)=\exp(-\alpha|\boldsymbol{r}-\boldsymbol{R}_A|^2) \tag{A5}$$

$$\chi_\nu(\boldsymbol{r}-\boldsymbol{R}_B)=\exp(-\beta|\boldsymbol{r}-\boldsymbol{R}_B|^2). \tag{A6}$$

Using (A5) and (A6) and standard mathematical tools [42], the general exact 'Madelung' matrix element (A4) becomes

$$\tilde{V}^{\mathrm{M}}_{\mu\nu}=-Q_C\frac{2\pi}{(\alpha+\beta)}\exp\left(-\frac{\alpha\beta}{(\alpha+\beta)}|\boldsymbol{R}_A-\boldsymbol{R}_B|^2\right)F[(\alpha+\beta)|\boldsymbol{R}_P-\boldsymbol{R}_C|^2] \tag{A7}$$

where

$$\boldsymbol{R}_P=(\alpha\boldsymbol{R}_A+\beta\boldsymbol{R}_B)/(\alpha+\beta) \tag{A8}$$

and

$$F[u]=\frac{1}{\sqrt{u}}\int_0^{\sqrt{u}}\exp(-t^2)\,\mathrm{d}t. \tag{A9}$$

The integral $F[u]$ converges rapidly for moderately large $\sqrt{u}$, i.e. for moderately large distances between point charge C and the midpoint of A and B, and approaches the limiting value $\sqrt{(\pi/4u)}$. Thus in this limiting case $\tilde{V}^{\mathrm{M}}_{\mu\nu}$ may be approximated by

$$\tilde{V}^{\mathrm{M}}_{\mu\nu}\simeq V^{\mathrm{M}}_{\mu\nu}=\left(\frac{\pi}{\alpha+\beta}\right)^{3/2}\exp\left(-\frac{\alpha\beta}{(\alpha+\beta)}|\boldsymbol{R}_A-\boldsymbol{R}_B|^2\right)\frac{-Q_C}{|\boldsymbol{R}_P-\boldsymbol{R}_C|}. \tag{A10}$$

Recalling that overlap matrix elements between primitive Gaussians are

$$S_{\mu\nu}=\left(\frac{\pi}{\alpha+\beta}\right)^{3/2}\exp\left(-\frac{\alpha\beta}{(\alpha+\beta)}|\boldsymbol{R}_A-\boldsymbol{R}_B|^2\right) \tag{A11}$$

we finally have

$$V^{\mathrm{M}}_{\mu\nu}=-\frac{Q_C}{|(\alpha\boldsymbol{R}_A+\beta\boldsymbol{R}_B)/(\alpha+\beta)-\boldsymbol{R}_C|}S_{\mu\nu}. \tag{A12}$$

Let us distinguish between two cases:

(i) $\boldsymbol{R}_B=\boldsymbol{R}_A$. This situation fixes the diagonal matrix elements. From (A12) we obtain

$$V^{\mathrm{M}}_{\mu\nu}=-(Q_C/|\boldsymbol{R}_A-\boldsymbol{R}_C|)\,S_{\mu\nu} \tag{A13}$$

which is identical to the expression (A1). Thus (A1) and hence (11*a*) are exactly fulfilled if $|\boldsymbol{R}_A-\boldsymbol{R}_C|$ is large.

(ii) $\boldsymbol{R}_B \neq \boldsymbol{R}_A$. This non-identity corresponds to the off-diagonal matrix elements, for which (A12) is the analytical limiting value. If, additionally, the two Gaussians have the same exponents $\alpha = \beta$, then

$$V_{\mu\nu}^{\mathrm{M}} = -\frac{Q_C}{|(\boldsymbol{R}_A + \boldsymbol{R}_B)/2 - \boldsymbol{R}_C|} S_{\mu\nu} \tag{A14}$$

which is identical to (A3). Thus (A3) and hence (11*b*) are exactly fulfilled for $|(\boldsymbol{R}_A + \boldsymbol{R}_B)/2 - \boldsymbol{R}_C|$ large and $\alpha = \beta$. If different Gaussians enter in (A12), then (A3) and hence (11*b*) contain an additional approximation. This approximation may be removed by evaluating the Madelung potentials at the centres of products of Gaussians ($\boldsymbol{R}_P$) rather than at midpoints between atoms. However, since the error is small and the correction had to be performed on the level of primitive Gaussians, i.e. at the price of considerable additional computational effort, we decided to use approximation (11*b*) instead of a 'weighted' variant.

References

[1] Born M and Landé A 1918 *Verhandl. Deut. Phys. Ges.* **20** 202
[2] Madelung E 1918 *Phys. Z.* **19** 524
[3] Boyer L L, Mehl M J, Feldman J L, Hardy J R, Flocken J W and Fong C Y 1985 *Phys. Rev. Lett.* **54** 1940
[4] Watson R E, Davenport J W, Perlman M L and Sham T K 1981 *Phys. Rev.* B **24** 1791
[5] Brédas J-L 1980 *Recent Advances in the Quantum Theory of Polymers* (*Lecture Notes in Physics 113*) ed J-M André, J-L Brédas, J Delhalle, J Ladik, G Leroy and C Moser (New York: Springer) p 92
[6] Ewald P P 1921 *Ann. Phys.* **64** 253
[7] Evjen H M 1932 *Phys. Rev.* **39** 675
[8] Emersleben O 1950 *Z. Angew. Math. Mech.* **30** 252
[9] Bertaut E F 1952 *J. Phys. Radium* **13** 499
[10] Metzger R M 1972 *J. Chem. Phys.* **57** 1870
[11] Pisani C and Dovesi R 1980 *Int. J. Quantum Chem.* **17** 501
[12] Wang Y, Nordlander P and Tolk N H 1988 *J. Chem. Phys.* **89** 4163
[13] Hoffmann R 1963 *J. Chem. Phys.* **39** 1397
[14] Weinberger P, Schwarz K and Neckel A 1971 *J. Phys. Chem. Solids* **32** 2063; Decicco P D 1967 *Phys. Rev.* **135** 931
[15] Rushan H, Gan Zizhao, Daole Y and Qing L 1990 *Phys. Rev.* B **41** 6683
[16] Del Re G, Ladik J and Biczó G 1967 *Phys. Rev.* **155** 997
[17] André J-M, Gouverneur L and Leroy G 1967 *Int. J. Quantum Chem.* **1** 427, 451
[18] Piela L and Delhalle J 1978 *Int. J. Quantum Chem.* **13** 605
[19] Delhalle J and Piela L 1980 *Phys. Rev.* B **22** 6254
[20] Harris F E 1975 *Theoretical Chemistry, Advances and Perspectives* vol 1, ed D Henderson and E Eyring (New York: Academic) pp 147–218
[21] Fripiat J G and Delhalle J 1979 *J. Comput. Phys.* **33** 425
[22] André J-M, Fripiat J G, Demanet Ch, Brédas J-L and Delhalle J 1978 *Int. J. Quantum Chem.* QCS **12** 233
[23] Delhalle J, Fripiat J G and Piela L 1980 *Int. J. Quantum Chem.* QCS **14** 431
[24] Mulliken R S 1955 *J. Chem. Phys.* **23** 1833
[25] Ladik J J 1988 *Quantum Theory of Polymers as Solids* (New York: Plenum) p 23
[26] Slater J C 1967 *Insulators, Semiconductors and Metals. Quantum Theory of Molecules and Solids* vol 3 (New York: McGraw-Hill) p 206
[27] Ziman J M 1972 *Prinzipien der Festkörpertheorie* (Zürich and Frankfurt: Harri Deutsch) p 39
[28] Mulliken R S 1949 *J. Chim. Phys.* **46** 497
[29] Löwdin P-O 1950 *J. Chem. Phys.* **18** 365
[30] Dovesi R, Pisani C, Roetti C and Saunders V R 1983 *Phys. Rev.* B **28** 5781
[31] Fleck O and Ladik J 1988 *Solid State Commun.* **65** 701
[32] Saalfrank P, Otto P and Ladik J 1989 *Solid State Commun.* **69** 99

[33] Dovesi R, Pisani C and Roetti C 1980 *Int. J. Quantum Chem.* **17** 517; Dovesi R, Pisani C, Roetti C and Dellarole P 1981 *Phys. Rev.* B **24** 4170
[34] Euwema R N, Surrat G T, Wilhite D L and Wepfer G C 1974 *Phil. Mag.* **29** 1033
[35] Zunger A and Freeman A J 1978 *Phys. Rev.* B **17** 2030
[36] Zunger A, Katzir A and Halperin A 1976 *Phys. Rev.* B **13** 5560
[37] Hehre W J, Stewart R F and Pople J A 1969 *J. Chem. Phys.* **51** 2657
[38] Gianolio R, Pavoni R and Clementi E 1978 *Gazz. Chim. Ital.* **108** 181
[39] Greuter F, Heskett D, Plummer E W and Freund H J 1983 *Phys. Rev.* B **27** 7117
[40] Zheng C, Apeloig Y and Hoffmann R 1988 *J. Am. Chem. Soc.* **110** 749
[41] Saalfrank P, Wood R F, Ladik J, Abdel-Raouf M A and Liegener C-M 1991 *Phys. Rev.* B submitted
[42] Szabo A and Ostlund N S 1989 *Modern Quantum Chemistry* (New York: McGraw-Hill) p 415